Investigating the accuracy of FatNav-derived estimates of temporal B_0 changes and their application to retrospective correction of high-resolution 3D GRE of the human brain at 7T

Frédéric Gretsch,[1] José P. Marques[2], Daniel Gallichan[3,4]

[1] Laboratory for Functional and Metabolic Imaging, École Polytechnique Fédérale de Lausanne, Lausanne, Switzerland

[2] Donders Institute, Radboud University, Nijmegen, the Netherlands

[3] Biomedical Imaging Research Center, École Polytechnique Fédérale de Lausanne, Lausanne, Switzerland

[4] Cardiff University Brain Research Imaging Centre (CUBRIC), School of Engineering, Cardiff University, Cardiff, UK

***Corresponding author:** E-mail frederic.gretsch@epfl.ch, Telephone: +41216930599

Abstract

Purpose: To investigate the precision of estimates of temporal variations of magnetic field achievable by double-echo fat image navigators (FatNavs), and their potential application to retrospective correction of 3D GRE-based sequences.

Methods: Both head motion and temporal changes of B_0 were tracked using double-echo highly-accelerated 3D FatNavs as navigators – allowing estimation of the temporal changes in low spatial order field coefficients. The accuracy of the method was determined by direct comparison to controlled offsets in the linear imaging gradients. Double-echo FatNavs were also incorporated into a high-resolution 3D GRE sequence to retrospectively correct for both motion and temporal changes in B_0 during natural and deep breathing. The additional scan time was 5 minutes (a 40% increase). Correction was also investigated using only the first echo of the FatNav to explore the trade-off in accuracy vs scan-time.

Results: Excellent accuracy (0.27 Hz, 1.57-2.75 Hz/m) was achieved for tracking field changes and no significant bias could be observed. Artefacts in the 3D GRE images induced by temporal field changes, if present, were effectively reduced using either the field estimates from the double-echo or the first-echo-only from the FatNavs.

Conclusion: FatNavs were shown to be an excellent candidate for accurate, fast and precise estimation of global field variations for the tested patterns of respiration. Future work will investigate ways to increase the temporal sampling to increase robustness to variations in breathing patterns.

Introduction

Sequences based on T_2^* contrast have demonstrated great usefulness to brain MRI for identification of various anomalies and conditions such as microbleeds and multiple sclerosis, but also quantitative estimates of physical properties[1–3]. Common sequences for T2* contrast, such as susceptibility weighted imaging and quantitative susceptibility mapping, typically require long (>20ms) echo times. While the use of ultra-high field magnets provides a significant boost to the resolution for an equivalent signal-to-noise ratio (SNR), it also unavoidably makes these gradient-echo based sequences more sensitive to uncontrolled phase evolution during the long echo times[4]. These phase variations stem from both static background magnetic field inhomogeneity, but also from dynamic events, such as breathing[5,6] or system drifts. Several attempts at quantifying and correcting these dynamic changes have been reported, using either navigator techniques[7–9] or external hardware[10–13]. Navigator methods at 7T which incorporate tracking the temporal B_0 variation in full 3D have yet to be demonstrated, although some hybrid methods went beyond a single dimension[14], where the sensitivity maps of the RF receive array were used to provide additional 2D in-plane spatial information to a one-dimensional projection. Ultra-high field also allows for high SNR very-high resolution (<0.5mm in plane) 3D acquisitions, but these necessarily imply longer acquisition times, thereby further increasing the probability of the scan being detrimentally affected by subject motion. Using parallel imaging[15,16] , highly accelerated fat selective navigators (FatNavs) have previously demonstrated the ability to quantitatively track motion and significantly improve image quality using either a retrospective[17] or a prospective[18] correction approach.

In this work we propose an extension of the FatNavs protocol to a double-echo acquisition. This approach allows mapping of the 3D dynamic B_0 variation in the fat layer, and to estimate the associated low order field coefficients. Adding the motion information, we also show that both effects can be retrospectively accounted for during image reconstruction, and that applying both of these corrections can result in a pronounced improvement in image quality for cases where these artifacts are strong.

Methods

All experiments were conducted on a 7T head-only MR scanner (Siemens Healthcare, Germany) using a 32-channel RF coil (Nova Medical Inc.). Two main experiments were conducted: The first aimed at quantifying the accuracy of the B_0 field estimates derived from the FatNavs. The second was a high-resolution 3D GRE scan, which will be referred to as the host sequence, into which FatNavs were inserted (~17 minutes). For the second experiment, volunteers were first asked to breathe deeply and slowly, after which a repetition of the scan was acquired, where this time they were asked to breathe in the way that seemed the most natural to them. Asking compliant volunteers to perform heavy deep breathing is expected to simulate the kinds of image artifacts that might arise from B_0 variations in less cooperative subjects or within certain patient populations.
We now introduce the necessary definitions and notations, and detail the protocols for the different experiments thereafter.

Retrospective correction of motion and temporal B_0 changes

We assume the motion can be well described by a rigid body transformation[19] $\boldsymbol{x}(t) = R(t)\boldsymbol{x_0} + \boldsymbol{d}(t)$, where R is a rotation matrix and $\boldsymbol{d}$ a translation vector. Keeping in mind the implicit time dependence of the various variables, including $\mathbf{k}$, the signal y measured in coil c at k-space position $\mathbf{k}$ is related to the non-moving object ρ by

$$\mathrm{y_c}(\mathbf{k}) = \int s_c(\boldsymbol{x})\rho(\boldsymbol{x}) \exp\left(-i2\pi\left[R\boldsymbol{k}\cdot(\boldsymbol{x}-\boldsymbol{d}) + \Delta B_0(\boldsymbol{x})\left(TE + \frac{k_{RO}}{G}\right)\right]\right) d^3\boldsymbol{x} \qquad (1)$$

where s_c is the receive coil sensitivity (assumed to be quasi-invariant under motion), TE is the echo-time, k_{RO} is the readout component of $\mathbf{k}$, and G is the readout gradient amplitude.

Neglecting phase accumulation during readout, only temporal variations of $\Delta B_0(\boldsymbol{x})$ induce image artifacts. Furthermore, these are generally well represented by low order spherical harmonics[8] . Approximating ΔB_0 to its first order components

$$\Delta B_0(\boldsymbol{x}, t) = \beta_0(t) + \boldsymbol{\beta}(t)\cdot\boldsymbol{x} \qquad (2)$$

allows for an efficient reconstruction using a nuFFT[20] operator with ten time-dependent parameters: six for motion and four for dynamic field variations. In k-space, β_0 and $\boldsymbol{d}$ contribute to a phase correction term, whereas R and $\boldsymbol{\beta}$ respectively amount to local rotations and shifts.

FatNav protocol and image reconstruction

The navigator protocol was a highly accelerated double-echo 3D GRE with a 1-2-1 binomial fat excitation pulse. It was chosen as a compromise between voxel size, phase evolution time and total acquisition time[21]. Parameters were: 3.94 mm isotropic resolution, 64x64x48 full matrix size, ¾ partial Fourier undersampling along both phase encode directions, FA = 5°, TE1 / TE2 / TR = 1.16 / 4.16 / 5.4 ms, readout bandwidth of 3910 Hz/pixel, and 4x4 GRAPPA acceleration, leading to a volume acquisition time of 583.2 ms. GRAPPA calibration lines were acquired separately as a prescan. An equivalent single echo FatNav would take 260 ms to acquire.

FatNav reconstruction was performed as follows: first, GRAPPA was applied to recover fully sampled k-space, from which square-root sum-of-squares (RSS) volumes of the first echo were co-registered using the *realign* tool in SPM (Statistical Parametric Mapping, version 12, registration parameters: 2 mm resolution interpolation, 3 mm smoothing window) to obtain motion estimates. Then, again from the fully sampled k-space, we directly reconstructed all channels c and echoes E for each volume using a nuFFT with the associated motion parameters. The resulting complex images $I_c(x, E)$ are therefore co-registered with the motion reference volume (the selection of which is explained below) directly in the image reconstruction. The final field map B_0 for a given volume was defined by

$$2\pi(TE_2 - TE_1)\Delta B_0(x) = arg\left(\frac{1}{N_c}\sum_{c=1}^{N_c}\frac{I_c(x,E_2)^*\, I_c(x,E_1)}{|I_c(x,E_2)|}\right) \qquad (3)$$

where N_c is the number of receive coils. The temporal variation of the B_0-field is readily obtained by a phase difference computation to a reference FatNav. The reference volume, for both motion and B_0, was chosen as the one acquired the closest to the host sequence k-space center in experiment 2, and as a fixed number larger than one (necessary for the magnetization to reach a steady state) in experiment 1. At no stage is any partial Fourier filter applied and the Fourier transform is taken after zero-padding. As the phase changes due to breathing are typically smoothly varying, we do not expect the reduction in spatial resolution due to partial Fourier undersampling to affect the fidelity of tracking these phase changes. We validated this assumption by acquiring

the same FatNav protocol but without any partial Fourier undersampling on one volunteer. We retrospectively down-sampled it and compared the estimated field change coefficients with and without partial Fourier undersampling.

The fit of the linear coefficients of temporal field variation was restricted to a fat-mask, defined by thresholding the reference volume first-echo RSS image. The threshold value was found by direct visual inspection and was the same for all volunteers.
This reconstruction pipeline gives direct access to the ten parameter time-courses used in the host sequence reconstruction. As expected, the field estimates obtained in this manner are still residually affected by subject motion – which has two main sources. The first is some inaccuracy of the applied method, such as incorrect motion estimation or limitations of the assumption of rigid-body motion. The second is the motion-induced change of the magnetic susceptibility spatial distribution relative to the static superconducting magnet, which in turn produces a change of the net magnetic field[22]. The results presented in this paper lead us to believe that the method is sufficiently accurate for our purposes, and consider the complete quantification of the induced field effect to be outside of the scope of this work.

We also note that the change of phase $\delta\varphi_{ci}$ of a single voxel for a given coil c and echo i can be modeled as

$$\delta\varphi_{ci} = \delta\phi_c + 2\pi\Delta B_0 TE_i \qquad (4)$$

where $\delta\phi_c$is the change of receiver phase due to motion and ΔB_0 is the local temporal variation of field. Therefore, in the case of negligible receive phase change, tracking temporal changes in the field rather than absolute values does not require the use of the second echo. Indeed, letting $I_{c,r}$ be the first echo image of the reference volume for the receive coil c, then the field variation map ΔB_0 can be defined as

$$2\pi TE_1\Delta B_0(x) = arg\left(\frac{1}{N_c}\sum_{c=1}^{N_c}\frac{I_c(x,E_1)^*\, I_{c,r}(x)}{|I_c(x,E_1)|}\right). \qquad (5)$$

Additionally, using both FatNav echoes it is also possible to derive a $\delta\phi_c$ map, allowing for a correction of the host data which incorporates both contributions to the temporal phase changes (changes in receiver phase as well as changes in B_0). However, we found that the magnitude of $\delta\phi_c$ was not large enough to make a noticeable difference in the corrected host data (see Appendix 1 for estimation of expected magnitude for $\delta\phi_c$). We therefore used Equation (3) for the dual-echo estimates of ΔB_0 and Equation (5) for single-echo estimates of ΔB_0– which is sufficient for the purposes of correcting the host data as the 'absolute' value of B_0 is not required.

Experiment 1: Determining the accuracy of field monitoring

In order to estimate the accuracy of the field monitoring, we acquired 72 consecutive FatNavs (after steady state was reached), where every other volume had a predetermined offset of one of the imaging gradients. In order to diminish the motion-related field changes which would reduce the apparent accuracy of the method, visual inspection of the motion parameters ensured that no large motion occurred during these acquisitions. These gradient offsets values were chosen in the (-50,50) Hz/m range. Due to time considerations, not all offsets values for all directions were acquired for each volunteer. However, a 20 Hz/m offset for each direction was always acquired for the four volunteers who completed this experiment to allow direct comparison between subjects. This corresponds approximately to the typical natural breathing range in the z direction at 7T. Using the same value for the x and y directions allows assessment of whether the method might also show some systematic anisotropy. Two different methods were investigated for estimation of the gradient offset amplitude and the associated error. Let $b_n\ n = 1, \dots, 2N$ be some field coefficient as defined in equation (2), where N is the number of control/offset volumes pairs. We constructed a sequence of field coefficient differences d_n which represents the measured field temporal variation. Two construction methods were investigated: the first method uses the consecutive volume difference (CVD) sequence $d_n = b_{2n} - b_{2n-1}\ ,\ n = 1, \dots, N$. It assumes the field change is exclusively due to the gradient current offset during the measurement time of this pair of volumes. However, residual breathing effects are bound to be captured as well, thereby diminishing the apparent precision of the offset estimate given by the CVD method. The second method, dubbed double linear interpolation difference (DLID), tries to evaluate consecutive FatNavs of the same kind (control or offset) at the same time point than the sandwiched FatNav (offset or control) before doing the difference. Mathematically the sequence studied is

$$d_n = \begin{cases} \frac{1}{2}(b_n + b_{n+2}) - b_{n+1}\ ,\ n\ odd \\ b_{n+1} - \frac{1}{2}(b_n + b_{n+2})\ ,\ n\ even \end{cases} \quad n = 1, \dots, 2N-2. \qquad (6)$$

Given the short volume acquisition time of the FatNavs, this method is assumed to interpolate any residual breathing-related field change, and thus allow a less biased statistical analysis (under the hypothesis of independent uniformly distributed noise realizations).

The accuracy of the method was defined from the root-mean-square-error (RMSE) of the error sequence given by $d_n - T$, where T is the known input offset (either zero or equal to the chosen linear offset). This RMSE is necessarily larger than the true precision of the method, as the following argument demonstrates. Let $b_i = p_i + T_i + \varepsilon_i$ with p_i the physiological contribution to the field change, T_i the offset (0 or the input offset), and ε_i the error. Assuming the sums of mixed terms of the form $p_i\varepsilon_j$ to be negligible, which is equivalent to the independence of the physiological field change and the noise realization, the RMSE of the DLID is given by

$$RMSE = \sqrt{\frac{1}{2N-2}\sum_{i=1}^{2N-2}\left[\frac{1}{2}(p_n + p_{n+2}) - p_{n+1}\right]^2 + \left[\frac{1}{2}(\varepsilon_n + \varepsilon_{n+2}) - \varepsilon_{n+1}\right]^2}. \quad (7)$$

White uncorrelated noise thereby implies $RMSE = \sqrt{\frac{3}{2} < \varepsilon^2 >}$ in the case of perfect physiological contributions suppression. In practice the suppression is certainly not perfect, and the RMSE is larger than the precision of the method itself. We define the field change coefficient precision, noted $\bar{\varepsilon}$, as

$$\bar{\varepsilon} = \sqrt{\frac{2}{3}}\, RMSE. \quad (8)$$

Experiment 2: High resolution T2* scans

The high resolution protocol was a 3D GRE transversal slab, with flow compensation in all directions, nominal resolution: 0.25x0.25x1.2 mm^3, full matrix size: 768x 672x64, ¾ partial Fourier undersampling in both phase encode directions, FA = 9°, TE / TR = 25 / 30 ms, receiver bandwidth = 220 Hz/pixel .
FatNavs were acquired between sequential k-space planes of the host sequence. This way, disruptions to the steady-state water signal are smoothly distributed in k-space along the innermost phase encoding loop direction, inducing only a slight blurring on the final image. Bloch simulations for these experimental parameters for white matter, gray matter and CSF (assumed T_1 = 1.15/1.9/4.47 s respectively) showed that the point-spread function of the water image is only marginally changed by the inclusion of the FatNavs. Its zero crossings by any practical measure are identical and the phase changes only outside of the first lobe. The resolution loss compared to the same scan without FatNavs is below 2%. Furthermore, contrast is barely affected: see Supporting Figure S1. The temporal resolution of the FatNavs was 2 s and the total acquisition time was 17min 2s, where the same GRE acquisition could have been performed in 12min 6s without the additional time needed for the FatNavs. Previous studies[23] showed that the average natural breathing period of the studied population lying in the supine position is slightly above 4 seconds. This means that while slow, deep breathing should be accurately sampled by the FatNavs, natural breathing is very close to the limit imposed by the FatNavs temporal resolution. We expect that partial sampling and partial correction can take place in this case (see Discussion for potential solutions to this limitation). The linear field coefficient fits of the FatNav B_0 maps were restricted to the host excitation slab, after fat identification by magnitude thresholding (as explained above). Reconstructions using no field, the zeroth (β_0 only) and first (β_0 and $\boldsymbol{\beta}$) order field corrections were performed separately for data from each receive coil and then combined using RSS. First-order correction based on field coefficients derived from (5) was also investigated.

Magnitude bias-field correction of the GRE images was performed by a point-wise division of the RSS image with a bias-field map. The bias-field map was found by smoothing a low-resolution version of the image, and interpolating the result back to the 3D GRE high-resolution grid. Quantification of image quality was evaluated using a gradient entropy metric (taking the sum of the image entropy of the finite differences of neighboring pixels in the x, y and z directions), as previous work[24,25] showed this metric to be a strong candidate as a surrogate marker for the subjective definition of what a “good” image is.

Results

Determining the accuracy of field monitoring

Retrospective partial Fourier down-sampling showed no significant change to the estimates of phase variations, as can be seen in Supporting Figure S2. The RMSE between with and without retrospective partial Fourier undersampling were 0.1 Hz for the 0^{th} order term, and 1.8 / 2.5 / 4 Hz/m for the x / y / z directions. Figure 1 illustrates the difference between the CVD and the DLID methods for a field offset of 5 Hz/m in the x direction, thus theoretically leaving only noise and breathing as contribution to the y and z field coefficients variations. Breathing is clearly observed (Figure 1 A. and B). The magnitude of the breathing-induced field change is in agreement with previously published values at 7T. The slight bias in the x direction due to the gradient offset cancels out when taking the mean across breathing peaks and troughs. These were found by extrema identification of the spatial mean B_0 value, computed in the fat layer mask using both FatNavs echoes. Because breathing contributes significantly to the error estimates (Figure 1 C) for the CVD method, but not for the DLID method, which shows a more homogeneous spectrum (as is expected for random noise), all the following results were obtained using the DLID method.

Quantitatively, the mean (maximum in brackets) precision $\bar{\varepsilon}$ across gradient offsets for $\beta_0, \beta_x, \beta_y, \beta_z$ were 0.29 (0.45) Hz, 1.57 (3.14) Hz/m, 2.35 (4.31) Hz/m and 2.75 (5.19) Hz/m respectively. As a current offset in one gradient should not influence the field estimates for the other two directions, these mean and maximum values include the precision of field estimates in these others directions. Measured shift values for all volunteers are shown in Figure 2. All estimates matched the target field shift (up to the first standard deviation) for the y and z directions, and one subject falls outside the first standard deviation for the x direction. The precision of the method shows no significant spatial anisotropy, reinforcing the absence of systematical bias in the method (by the choice of phase encoding directions for example).

Similarly, the precision values using only the first echo of the FatNavs (equation (4)) for $\beta_0, \beta_x, \beta_y, \beta_z$ were 0.44 (0.91) Hz, 2.63 (5.74) Hz/m, 5.24 (15.79) Hz/m and 4.18 (11.22) Hz/m respectively. These values are approximately double the precision of the dual-echo estimates.

High resolution T2* scans

A representative slice of the high-resolution 3D GRE scans while breathing slowly and deeply are shown in Figure 3 , for all investigated reconstructions. The sharpness of anatomical features is noticeably improved after motion correction. However, the large-scale ghosting and blurring artefacts typically induced by breathing are not suppressed. Incorporating correction of temporal magnetic field variations greatly reduces these artefacts, and first order correction further enhances image quality compared to the zeroth order correction. The six motion and four dual-echo field parameters derived from the FatNavs for this scan are shown in Figure 4. Figure 5 shows the parameters of volunteer 2 deep-breathing scan, where significant field variation induced by breathing also occurs along the y direction, indicating the utility of measuring the field variations using more than one-dimensional projection in such cases.

Similarly, representative results of scans where the subject was asked to breathe naturally are presented in Figure 6 , and the corresponding motion and field parameters in Figure 7. Similar levels of improvement following motion-correction were observed as in the deep-breathing experiment – with the improvement even more striking in Volunteer 1 due to the larger motion during that scan. Notice also that the field coefficients are also affected by motion, even though these are defined in the co-registered FatNav-space. This is most clearly seen when sudden motion takes place in Figure 7. While overall it is difficult to identify clear improvements to the image quality when the field variations are corrected for, increasing the number of correction parameters did show increasing image quality for volunteer 1 (this volunteer is also the one who moved the most). These results suggest that for healthy compliant subjects, and under the imaging parameters used in this experiment, breathing artifacts are typically not sufficiently severe for the correction to make a noticeable improvement. It is also plausible that breathing is not well sampled throughout the whole scan, leading to sub-optimal corrections (see Figure 7).

Comparison of typical slices in the deep breathing scan for the first-order field correction using dual-echo estimates (equation (3)) or the single-echo estimates (equation (4)) is shown in Figure 8 . The image quality of both reconstructions is very similar, and areas of subjectively 'better' image quality can be found in either reconstruction. As Figure 9 shows, the differences between the first-echo and dual-echo field estimates are largely explained by a simple first-order regression in the motion parameters. This in turn implies that in case of a drift-like motion, the phase terms for image corrections will differ by a drift as well, producing slightly shifted corrected images. Figure 10 shows the reduction of gradient image entropy between the raw reconstruction and the different corrections studied, normalized to the raw reconstruction value. We observe a decreasing gradient entropy (compared to the raw reconstruction) as higher order field terms are taken into accounts. The change is more pronounced for the deep breathing scan, as expected. The differences between first-echo and dual-echo based corrections are inconsistent across scans and volunteers (comparison shown for motion-correction and

B_0-correction up to 1st-order), but the gradient entropies following both these corrections were all lower than from the lower-order corrections.

Discussion

Determining the accuracy of field monitoring

We have developed a new method to study the robustness of estimates of linear field variations. High quality quantification of first-order dynamic field variation was achieved by the dual-echo field estimates. The associated variabilities (RMSE) were significantly lower than the typical range of variation observed due to breathing. The spatial distribution of the field variations due to breathing was also directly observed in the fat layer and agrees well with previous literature with measurements from the brain[5].

In the direct volunteer comparison (Figure 2), one of the estimates falls outside one standard deviation of the known value in the x direction. Despite this residual bias, correction using these estimates is expected to be better than no correction at all – and this minor overestimation (in one subject by up to ~15%) is not expected to appreciably affect the level of correction achievable, especially as this was only observed for a gradient in the x direction where the effect due to breathing is the lowest.

The advantage of alternating reference and offset volumes is that residual motion-induced phase variation is greatly reduced. Indeed, a phase difference of two volume-trains, one of reference volumes and one with field offset volumes, would be strongly influenced by any motion occurring during the acquisition. Only fast and large motion would influence (and artificially diminish) the estimated precision of the DLID method for a given gradient offset. For all volunteers in this study, we could always find a subset of 36 consecutive volume pairs for which no such larger motion took place. Another possibility for estimating the accuracy of the method independently from the physiological phase variations could have been to perform the experiment with breath-holding. However, due to the practical problems of breath-holding, such as good and constant subject cooperation, as well as decreased subject comfort, we think the DLID method, which gave reliable results during free breathing, is a good choice. The remaining limitations of the DLID method imply that the precision estimated in this experiment should be understood as an upper bound for the true precision of the parameter estimation, as DLID is expected to overestimate the true value. This experiment shows that double-echo FatNavs are well suited for accurate, fast low-order dynamic field tracking.

First-echo based field estimates suffer greatly from the associated loss of SNR compared to dual-echo estimates due to the shorter phase evolution period. The accuracy is reduced by a factor of approximately 1.5 to 2. While having a longer echo time would allow for better accuracy, it may be more sensible to acquire several echoes due to the short readout acquisition time.

High resolution T2* scans

In the deep and slow breathing experiments, image quality was always greatly improved by incorporating correction for the temporal variation of the magnetic field. Furthermore, the first order correction demonstrated additional improvement in the reconstruction quality over the zeroth-order correction, demonstrating the utility of accounting for the spatial dependence of temporal field variation at ultra-high field. This dependence is not necessarily restricted to the z direction and hence a true 3D quantification can be necessary. This is achieved by the dual-echo FatNavs but not previous navigator methods at 7T, which typically only focus on the z direction or use approximations to recover some spatial information from projections[14]. These methods also typically neglected motion entirely.

The high quality of the reconstructed images suggests that the motion and field parameters were well captured by the FatNavs. Clear impact of motion on the estimated field coefficients can also be seen, but the degree to which these are due to a true physical effect, such as magnetic susceptibility distribution change, or due to methodology errors cannot easily be estimated from this data. The consistent observation that the inclusion of each additional set of corrective parameters in Figure 3 leads to additional improvements in image quality implies that the observed interdependence of motion and field parameters is likely to have a true physical origin rather than being due to erroneous or incomplete modelling.

In the natural breathing case, the benefits of B_0 correction are marginal, and a clear difference between zeroth and first order corrections could only be observed in one subject. While areas of more homogenous contrast in the same tissue after field correction can be found, it is doubtful that these differences would be worth the additional scan-time inherent to the second-echo of the FatNavs. However, previously published results are unclear about the percentage of 3D GRE scans which would show natural breathing artefacts. Breathing itself is very person-specific. Also, the impact of thoracic breathing on the field variation spatial distribution is expected to be different than that of diaphragmatic breathing, due to different air distribution changes[22]. All-in-all, almost all regimes (breathing type, depth and frequency) could certainly be found within the normal range of 'natural breathing' by some individuals. Specific populations can also be more prone to exhibit significant field change, such as Alzheimer's patients[26]. This makes reaching a definitive claim on the usefulness of correcting for breathing-induced field variation very challenging. The method proposed here is shown to make a clear improvement in image quality for a specific sequence and in subjects with a specific breathing profile. Longer

echo times would also make the artefact worse for the same breathing pattern. All these considerations necessarily mean that the presented results of double-echo FatNavs inclusion in high-resolution 3D GRE are very much exploratory, but it also shows their usefulness in extreme cases.
It might be expected that the field in the fat layer could be more sensitive to motion than at the center the brain. The fat signal is very close to the large magnetic susceptibility change of the air-tissue boundary and this could lead to local changes in the field in the vicinity of the fat layer that are not reflective of the changes occurring in the center of the brain. This in turn would imply an overestimation of the field change given by the FatNavs compared to the true change in the brain. We observed a good correspondence in this study between the measured field changes and the subsequent improvements in image-quality when these estimates were used for correction, suggesting that over-estimation of motion-induced field changes in the fat layer was not a major problem in this study. We expect that discrepancies between field changes measured at the fat layer and real field changes in the brain could explain some of the residual artifacts present in the corrected images.
The GRE protocol used in this experiment was made ~40% longer due to the addition of the dual-echo FatNavs. Using only the first echo of the FatNavs for first-order field change correction appears to perform as well as the dual-echo derived correction when assessing the overall final image quality, but would greatly reduce the additional scan-time inherent to the navigators. Each FatNav would be 324 ms shorter, reducing the additional scan-time to ~18% of the original GRE protocol duration.

The difference between dual-echo and single echo field estimates is strongly correlated to the motion parameters. This likely arises from the fact that the dual-echo estimates remove the phase change under motion of the receive coil sensitivities, whereas the single echo estimates do not (see Appendix 1). This also means that the field change correction terms are *a priori* highly biased by motion because of the short FatNavs echo time, and we are currently investigating the reasons why this bias does not seem to produce additional artifacts in the reconstructions. In this study we found that quantifying image quality was very difficult – and although the reconstructed images corrected using single or dual-echo field estimates are measurably *different*, it is not clear which image is *better*. Unlike standard point-wise based image difference metrics which would be sensitive to image shifts, gradient image entropy shows the consistent trend that the image quality continues to increase as more correction parameters are used. However, it is insufficient to help us understand which of the dual-echo or first echo based correction is best. Future work will investigate whether a metric can be found that allows a more accurate reflection of the final image quality.
The most direct way to increase the temporal resolution of the FatNavs is to segment the host sequence acquisition and acquire a FatNav between each segment. Single-echo FatNavs in a 2-segment host sequence would be a way to double the FatNavs temporal resolution, while keeping the total scan-time equivalent to the one presented in this study. Previous conclusions suggest that the correction quality would be at least as good as the one presented here. Alternatives which do not add any additional scan-time, such as combination of FID navigators (one per host sequence shot) and FatNavs are also currently being explored, but go beyond the scope of this paper. The field change quantification method presented here can also be directly used for fitting coefficients of higher order than only the first-order terms. The restriction to the first spatial order was chosen solely because it allows for a much more time-efficient retrospective correction, as the linear terms correspond to simple shifts of k-space points. Inclusion of higher-order terms would require the use of more computationally intensive iterative reconstruction techniques[27]. However, it is likely to remain difficult to assess whether the increased computational burden is justified without a reliable corresponding metric for image quality.

Conclusions

This work shows that extending the previously proposed 3D FatNavs to a double-echo version allows to capture magnetic field temporal variations with excellent precision. Both motion and field variations (up to first order spatially) can be included in a retrospective correction of the full 3D k-space. For strong artifacts caused by heavy breathing this correction can provide substantial enhancement to the final image quality. Single echo estimates based corrections showed comparable results, and hence should allow a significant reduction of the additional scan-time due to the FatNavs second echo. The temporal sampling of the FatNavs in the current implementation is on the limit of critical sampling for normal healthy breathing rates. Future work will investigate approaches to increase the temporal resolution of the FatNavs, without sacrificing spatial resolution and fidelity, to be applicable to more general breathing patterns.

Acknowledgments

This work was supported by Centre d'Imagerie BioMédicale (CIBM) of the UNIL, UNIGE, HUG, CHUV, EPFL and the Leenaards and Jeantet Foundations, as well as the Swiss National Foundation through Grant 205321_153564.

Appendix 1 – Estimation of change in coil phase due to subject motion

We can estimate the local change in coil phase at a particular position within the head, $\delta\phi_c$, for some moderate motion δx as $\delta\phi_c = \frac{2\pi}{L}\delta x$ where L is the distance over which the phase changes by one full cycle. As a first approximation, we can use the RF wavelength as an estimate of L. The receive phase variation can be considered negligible when the ΔB_0 term in Equation 4 dominates, which can be formulated as when $2\pi\Delta B_0 TE \gg \delta\phi_c$, which corresponds to the condition $\Delta B_0\ TE\ \lambda \gg \delta x$. Assuming a typical value for ΔB_0 (1 Hz) and 20cm for λ, leads to $\delta x[mm] \ll 0.2\ TE[ms]$. This shows that, for long echo time, such as the ~25 ms TE used in the host sequence, the $\delta\phi_c$ term is negligible for motion up to around 5 mm (and indeed it was neglected in Equation (1)).

However, in the case of large motion and short echo-times, the estimates given by Equation (5) are expected to contain significant bias – which can be exacerbated by the short echo-times used for the FatNav. A single-echo FatNav might therefore falsely attribute a fraction of the measured phase changes to being due to changes in B_0 – as it will also be sensitive to $\delta\phi_c$. This is why in this study we compared the estimated correction terms from the first-echo of the FatNav against those from dual-echo – as well as comparing the effect this has on the corrected images themselves – to test whether a single-echo FatNav would be sufficient for the chosen sequence parameters.

References

1. Haacke EM, Liu S, Buch S, Zheng W, Wu D, Ye Y. Quantitative susceptibility mapping: Current status and future directions. Magnetic Resonance Imaging. 2015;33(1):1–25.

2. Chavhan GB, Babyn PS, Thomas B, Shroff MM, Haacke EM. Principles, techniques, and applications of T2*-based MR imaging and its special applications. Radiographics : a review publication of the Radiological Society of North America, Inc. 2009;29(62983):1433–1449.

3. Haacke EM, Mittal S, Wu Z, Neelavalli J, Cheng YCN. Susceptibility-weighted imaging: Technical aspects and clinical applications, part 1. American Journal of Neuroradiology. 2009;30(1):19–30.

4. Wen J, Cross AH, Yablonskiy DA. On the role of physiological fluctuations in quantitative gradient echo MRI: Implications for GEPCI, QSM, and SWI. Magnetic Resonance in Medicine. 2015;73(1):195–203.

5. Van de Moortele P-F, Pfeuffer J, Glover GH, Ugurbil K, Hu X. Respiration-inducedB0 fluctuations and their spatial distribution in the human brain at 7 Tesla. Magnetic Resonance in Medicine. 2002;47(5):888–895.

6. Raj D, Paley DP, Anderson a W, Kennan RP, Gore JC. A model for susceptibility artefacts from respiration in functional echo-planar magnetic resonance imaging. Physics in medicine and biology. 2000;45(12):3809–3820.

7. Bolan PJ, Henry P-G, Baker EH, Meisamy S, Garwood M. Measurement and correction of respiration-Inducedb0 variations in breast1h mrs at 4 tesla. Magnetic Resonance in Medicine. 2004;52(6):1239–1245.

8. Zahneisen B, Assländer J, Levan P, Hugger T, Reisert M, Ernst T, Hennig J. Quantification and correction of respiration induced dynamic field map changes in fMRI using 3D single shot techniques. Magnetic Resonance in Medicine. 2014;71(3):1093–1102.

9. Henry PG, Van De Moortele PF, Giacomini E, Nauerth A, Bloch G. Field-frequency locked in vivo proton MRS on a whole-body spectrometer. Magnetic Resonance in Medicine. 1999;42(4):636–642.

10. Duerst Y, Wilm BJ, Wyss M, Dietrich BE, Gross S, Schmid T, Brunner DO, Pruessmann KP. Utility of real-time field control in T2 *-Weighted head MRI at 7T. Magnetic resonance in medicine. 2015;22(April):312.

11. Duerst Y, Wilm BJ, Dietrich BE, Vannesjo SJ, Barmet C, Schmid T, Brunner DO, Pruessmann KP. Real-time feedback for spatiotemporal field stabilization in MR systems. Magnetic Resonance in Medicine. 2015;73(2):884–893.

12. Van Gelderen P, De Zwart JA, Starewicz P, Hinks RS, Duyn JH. Real-time shimming to compensate for respiration-induced B0 fluctuations. Magnetic Resonance in Medicine. 2007;57(2):362–368.

13. Vannesjo SJ, Wilm BJ, Duerst Y, Gross S, Brunner DO, Dietrich BE, Schmid T, Barmet C, Pruessmann KP. Retrospective correction of physiological field fluctuations in high-field brain MRI using concurrent field monitoring. Magnetic Resonance in Medicine. 2015;73(5):1833–1843.

14. Versluis MJ, Sutton BP, de Bruin PW, Börnert P, Webb AG, van Osch MJ. Retrospective image correction in the presence of nonlinear temporal magnetic field changes using multichannel navigator echoes. Magnetic Resonance in Medicine. 2012;68(6):1836–1845.

15. Pruessmann KP, Weiger M, Scheidegger MB, Boesiger P. SENSE: Sensitivity encoding for fast MRI. Magnetic Resonance in Medicine. 1999;42(5):952–962.

16. Griswold MA, Jakob PM, Heidemann RM, Nittka M, Jellus V, Wang J, Kiefer B, Haase A. Generalized Autocalibrating Partially Parallel Acquisitions (GRAPPA). Magnetic Resonance in Medicine. 2002;47(6):1202–1210.

17. Gallichan D, Marques JP, Gruetter R. Retrospective correction of involuntary microscopic head movement using highly accelerated fat image navigators (3D FatNavs) at 7T. Magnetic Resonance in Medicine. 2015;0:1–10.

18. Skare S, Hartwig A, Mårtensson M, Avventi E, Engström M. Properties of a 2D fat navigator for prospective image domain correction of nodding motion in brain MRI. Magnetic resonance in medicine. 2015;73(3):1110–9.

19. Zaitsev M, Maclaren J, Herbst M. Motion artifacts in MRI: A complex problem with many partial solutions. Journal of Magnetic Resonance Imaging. 2015;42(4):887–901.

20. Fessler JA, Sutton BP. Nonuniform fast fourier transforms using min-max interpolation. IEEE Transactions on Signal Processing. 2003;51(2):560–574.

21. Gallichan D, Marques JP. Optimizing the acceleration and resolution of three-dimensional fat image navigators for high-resolution motion correction at 7T. Magnetic Resonance in Medicine. 2017;77(2):547–558.

22. Marques JP, Bowtell R. Application of a fourier-based method for rapid calculation of field inhomogeneity due to spatial variation of magnetic susceptibility. Concepts in Magnetic Resonance Part B: Magnetic Resonance Engineering. 2005;25(1):65–78.

23. Avbelj V, Kalisnik J-M, Trobec R, Gersak B. Breathing rates and heart rate spectrograms regarding body position in normal subjects. Computers in biology and medicine. 2003;33(3):259–66.

24. Loktyushin A, Nickisch H, Pohmann R, Schölkopf B. Blind retrospective motion correction of MR images. Magnetic Resonance in Medicine. 2013;70(6):1608–1618.

25. McGee KP, Manduca A, Felmlee JP, Riederer SJ, Ehman RL. Image metric-based correction (Autocorrection) of motion effects: Analysis of image metrics. Journal of Magnetic Resonance Imaging. 2000;11(2):174–181.

26. Versluis MJ, Peeters JM, van Rooden S, van der Grond J, van Buchem MA, Webb AG, van Osch MJP. Origin and reduction of motion and f0 artifacts in high resolution T2*-weighted magnetic resonance imaging: Application in Alzheimer's disease patients. NeuroImage. 2010;51(3):1082–1088.

27. Wilm BJ, Barmet C, Pavan M, Pruessmann KP. Higher order reconstruction for MRI in the presence of spatiotemporal field perturbations. Magnetic Resonance in Medicine. 2011;65(6):1690–1701.

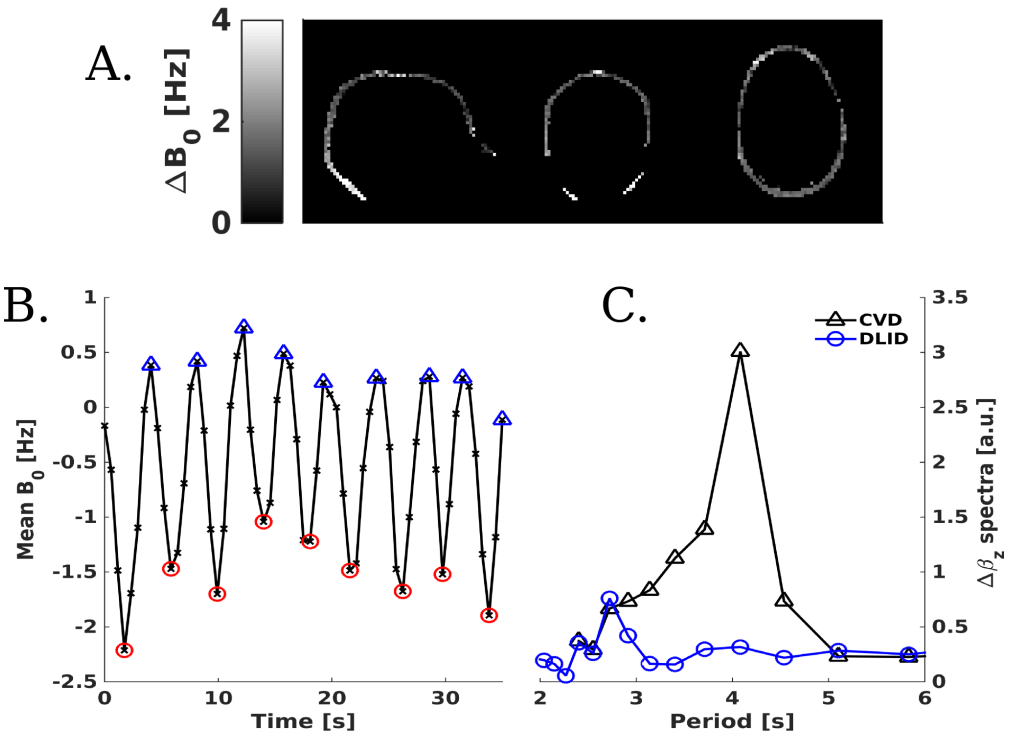

Figure 1: Example data from a single subject with a 5 Hz/m offset in the x direction every other volume. (A) Mean B0 difference between breathing peaks and troughs in the fat layer, after masking for fat signal. (B) Mean B0 field across entire fat signal mask vs time. Markers represent the peaks and troughs of respiration, used to derive the plot (A). (C) Spectra of the time-courses of the estimated linear field change in z derived from both consecutive volume difference (CVD) and double linear interpolation difference (DLID) methods, in arbitrary units [a.u.].

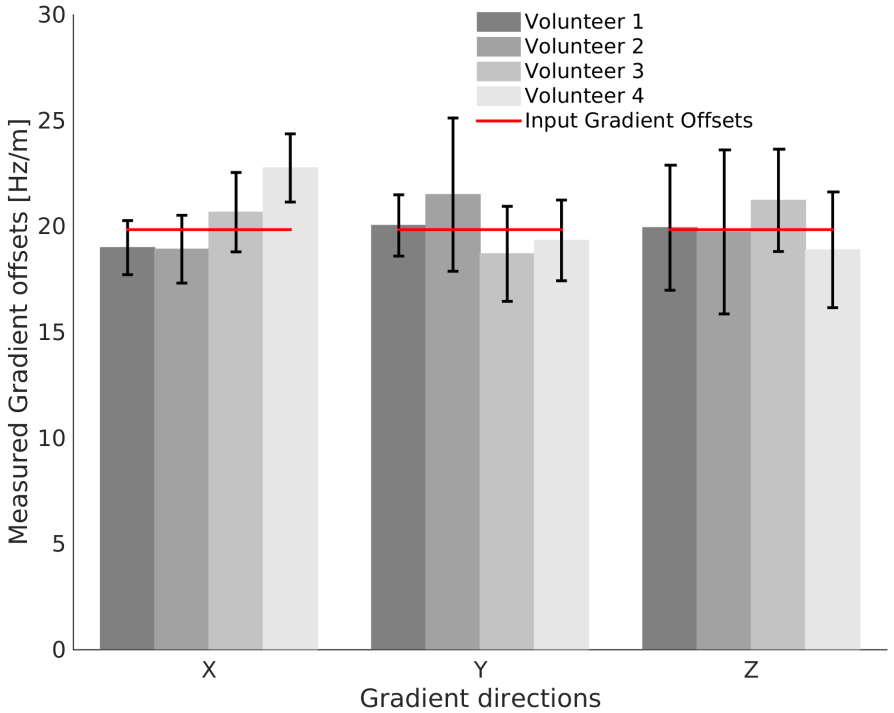

Figure 2: Gradient offsets measured across volunteers. Error bars show +- 1 standard deviation.

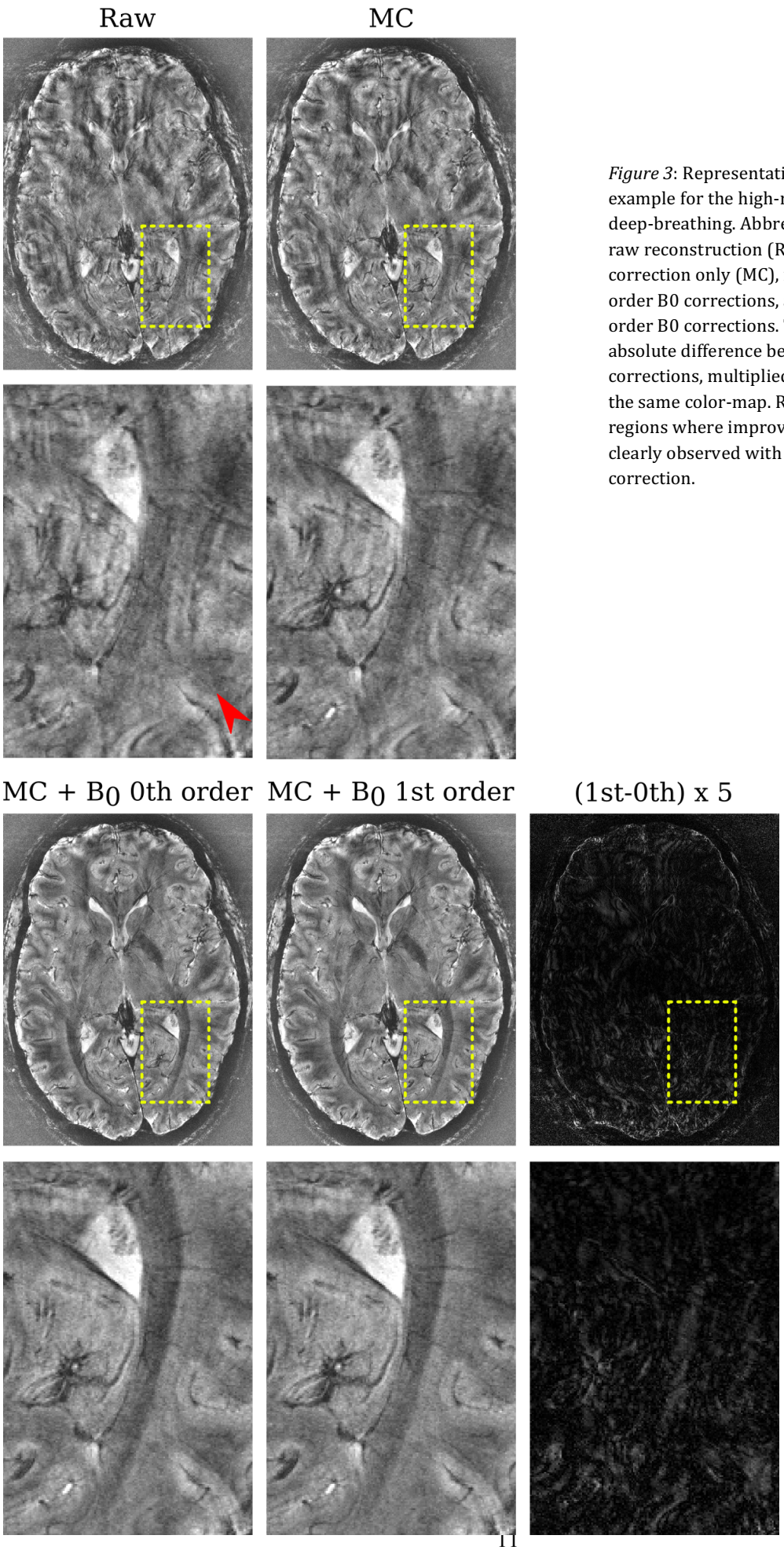

Figure 3: Representative reconstructions example for the high-resolution scan while deep-breathing. Abbreviations stand for: raw reconstruction (Raw), motion correction only (MC), motion and zeroth order B0 corrections, and motion and first order B0 corrections. The bottom right is the absolute difference between both B0 order corrections, multiplied by 5. All images use the same color-map. Red arrows highlight regions where improvements can be most clearly observed with increasing levels of correction.

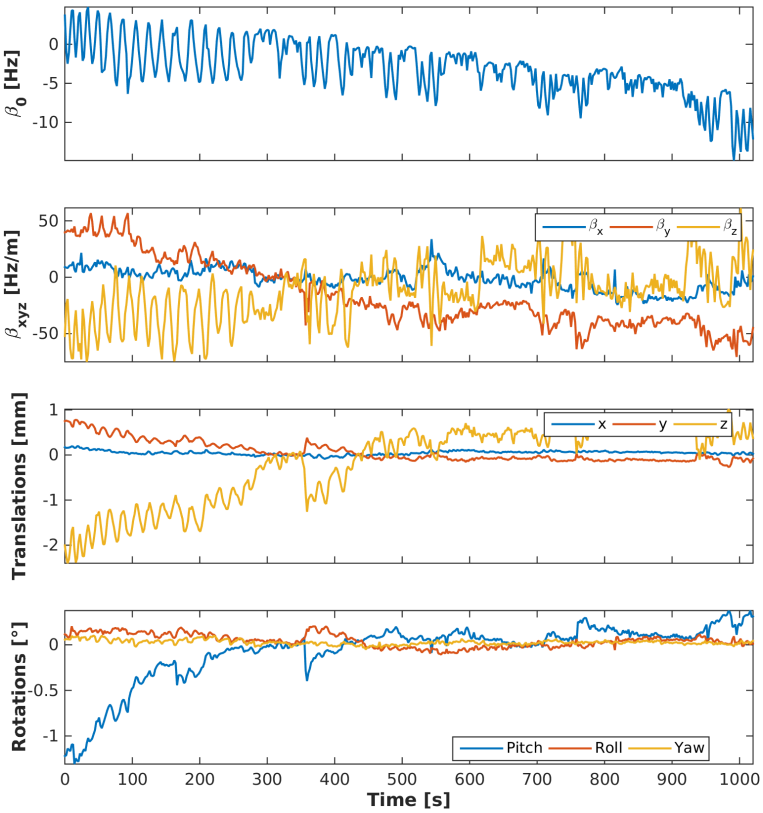

Figure 4: Estimated motion and field parameters for the scan of Figure 3 (volunteer 4), where the volunteer was asked to breathe deeply.

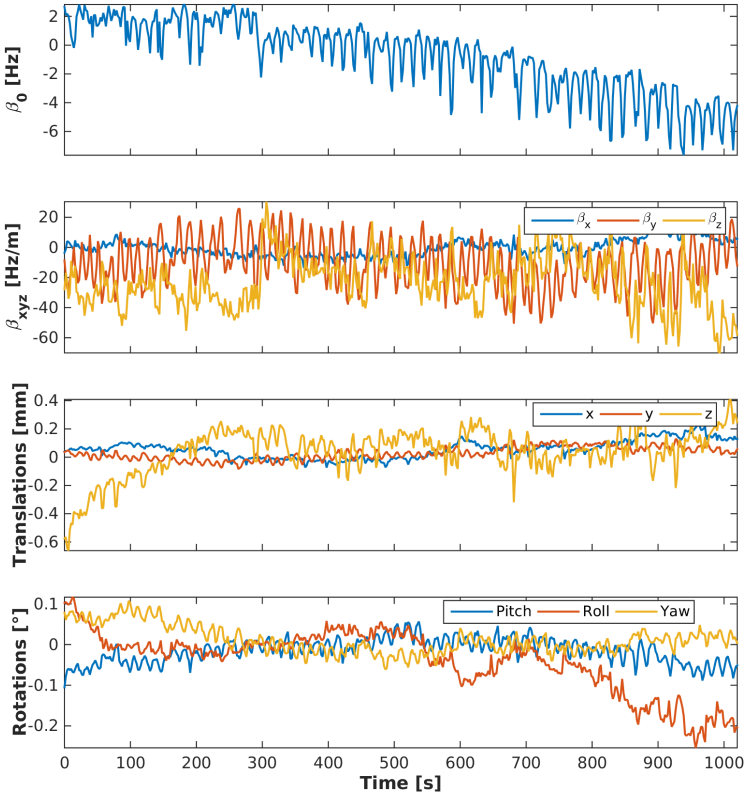

Figure 5: Estimated motion and field parameters for the deep breathing scan of volunteer 2.

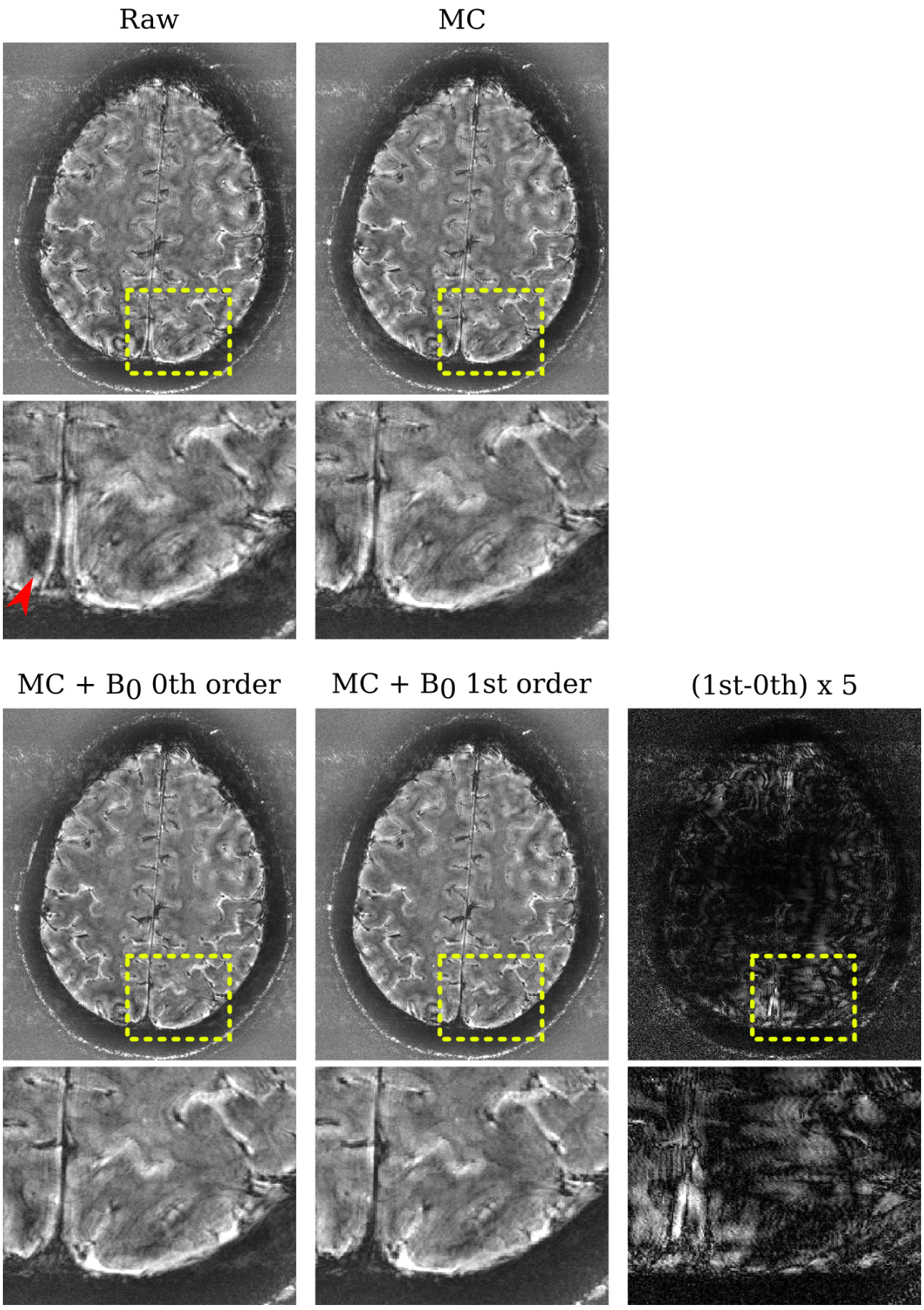

Figure 6: Representative reconstructions example for the high-resolution scan while subject breathed naturally. Figure organization is as in Figure 3.

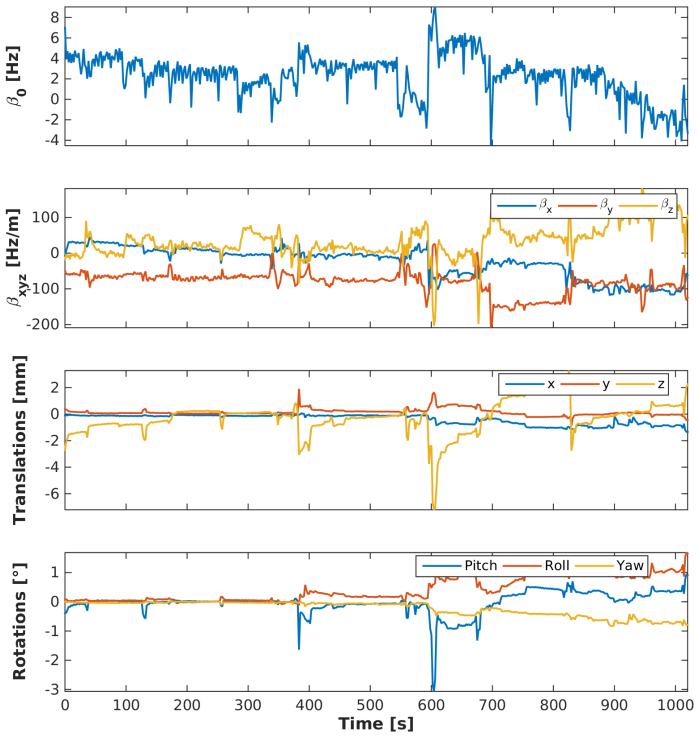

Figure 7: Estimated motion and field parameters for the scan of Figure 3 (volunteer 1), where the volunteer was asked to breathe normally.

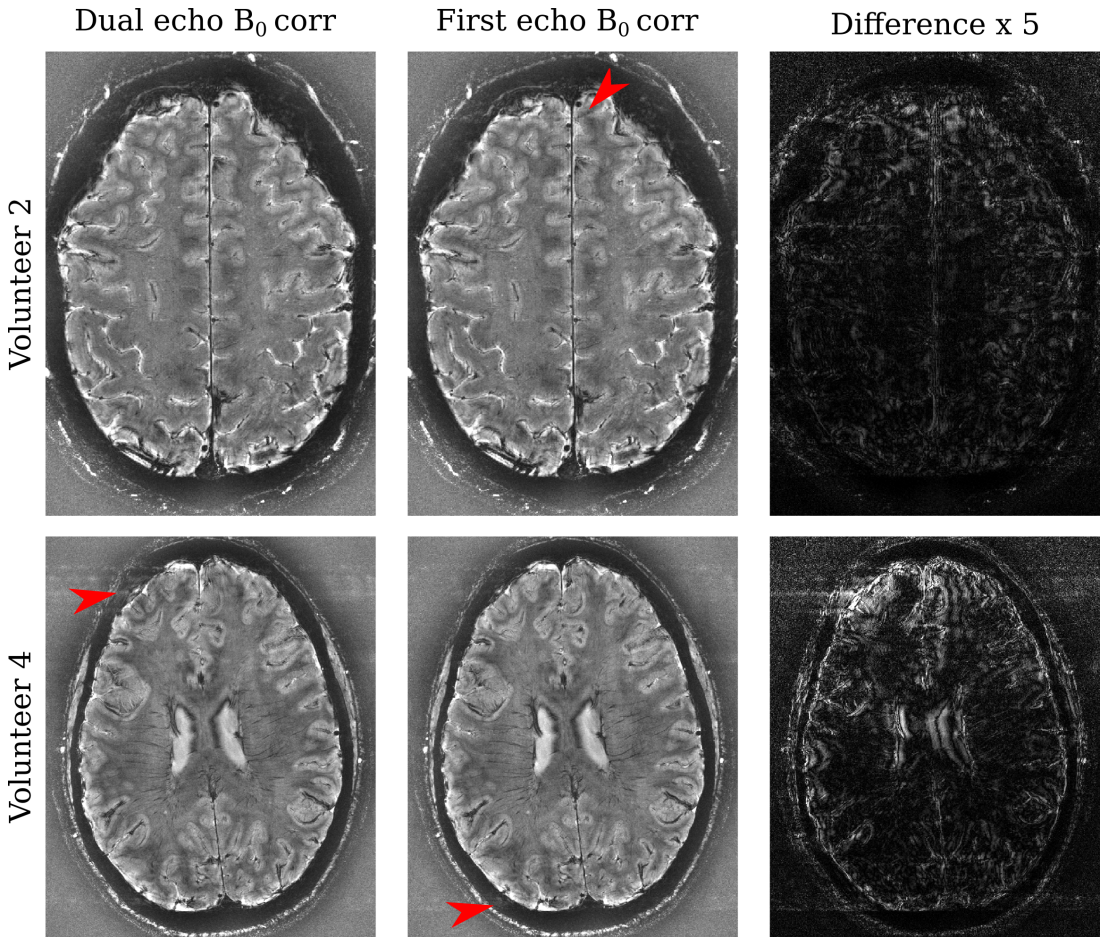

Figure 8: Representative motion and first-order B0 corrected images in the deep-breathing scan. First column is using both echoes from the FatNavs to estimate the field changes, whereas the second column uses only the first echo. The third column is the absolute difference times 5. Red arrows indicate regions where slight depreciative change of image quality can be found compared to the image without the red arrow.

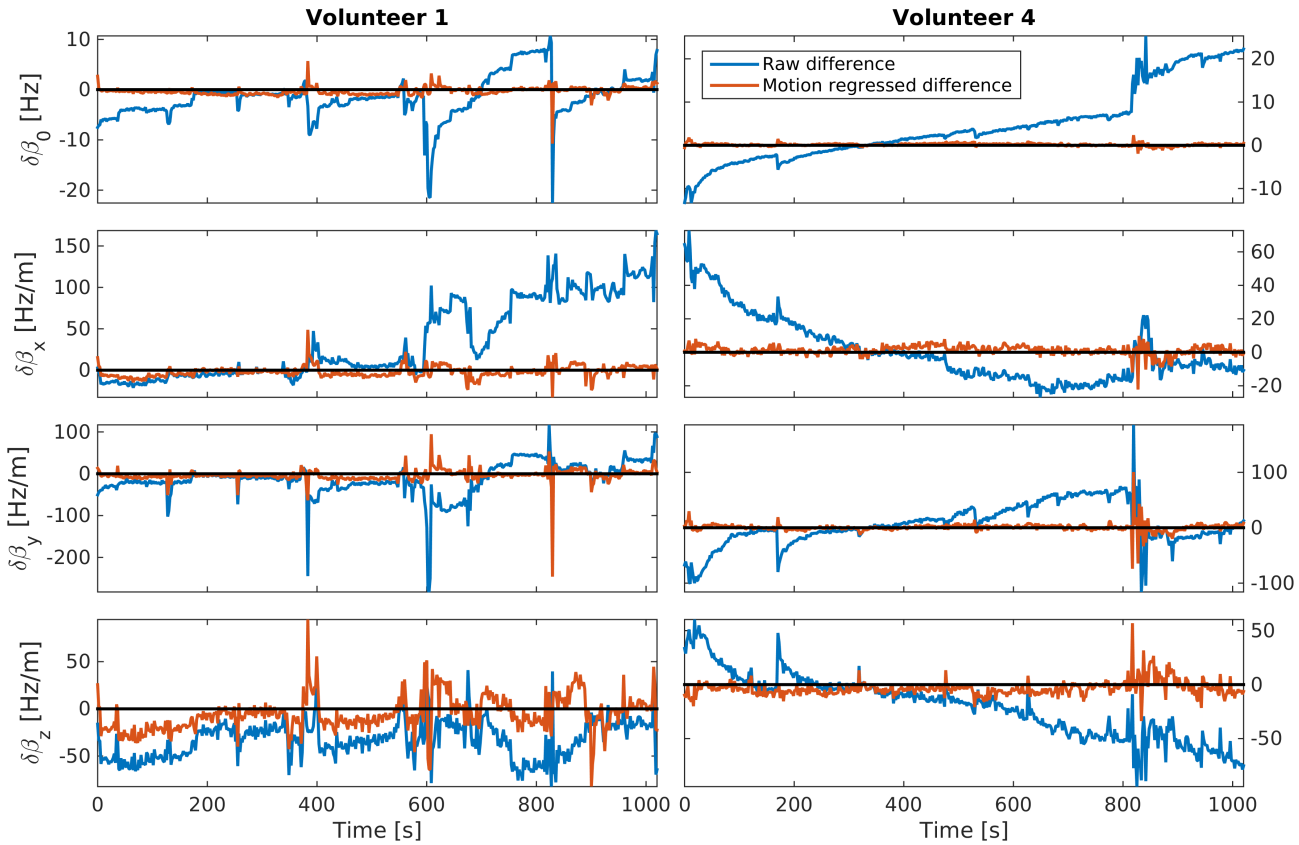

Figure 9: Difference between the dual-echo and first echo field coefficient estimates. The scans shown are those where the volunteers moved the most (both during the natural breathing scan). Both the raw difference and the first-order motion-regressed difference are shown. The horizontal black lines represent the constant zero value.

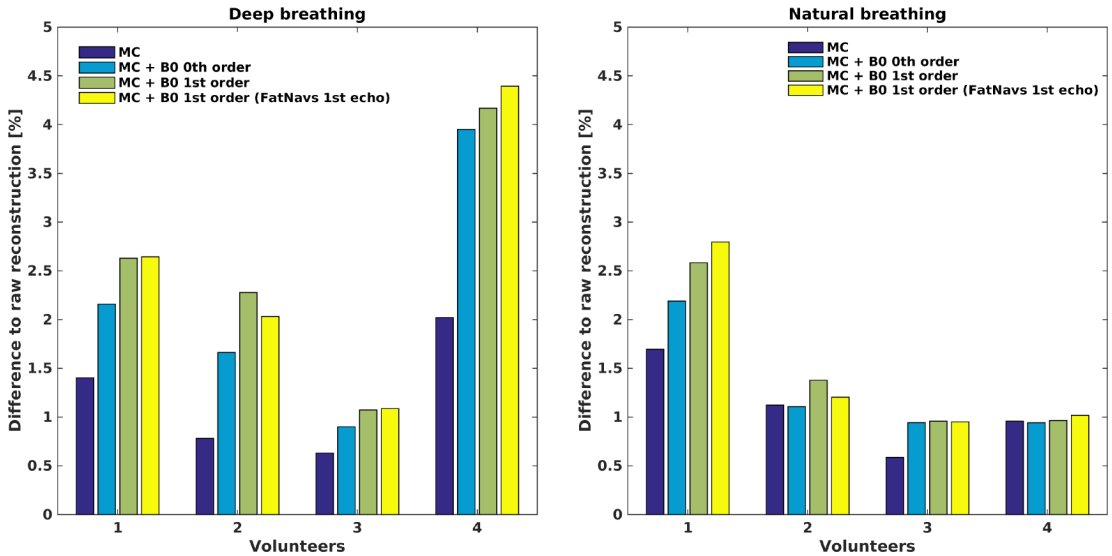

Figure 10: Bar plots showing the relative reduction of image gradient entropy between the raw images and the different corrected images for both deep breathing and natural breathing scans.

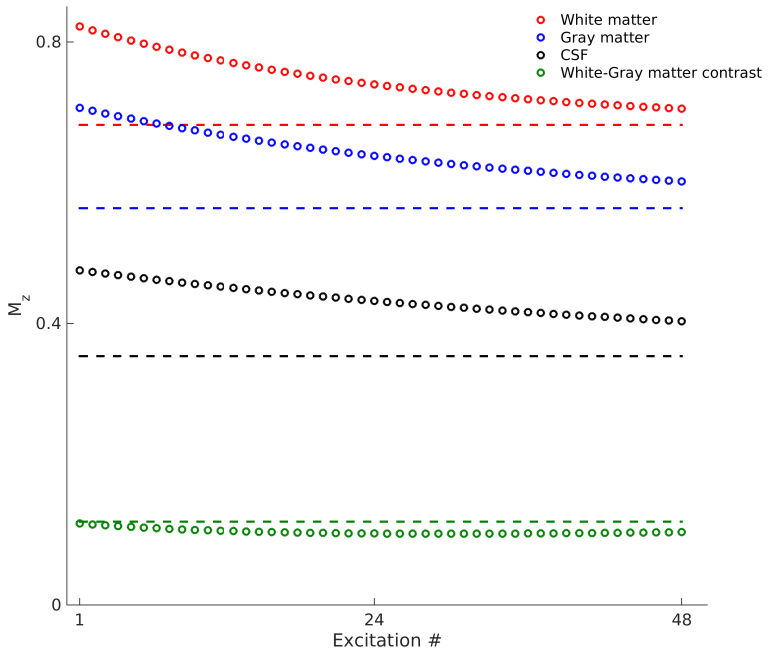

Supporting Figure S1: Bloch simulation of the water signal during the high-resolution GRE protocol with FatNav inclusion. Dashed lines represent the steady state in absence of FatNavs. The green line is the white to gray matter contrast. The point-spread functions associated to these signals are found by zero-padding and shifting before taking the Fourier transform to account for the host sequence partial Fourier. They show a resolution loss of less than 2.2%.

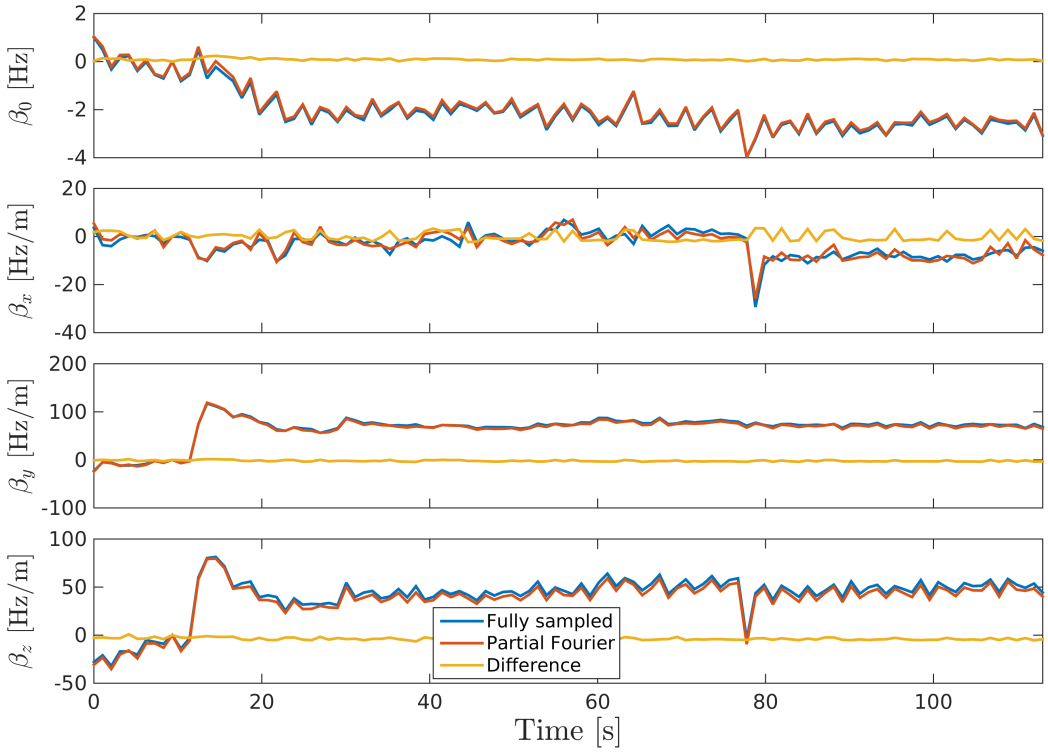

Supporting Figure S2: FatNavs without gradient offsets or partial Fourier were acquired. Field change coefficients were estimated using both all the measured data, or after partial Fourier simulation (in x and y). The RMSE between fully-sampled and partial Fourier reconstructions are 0.1 Hz for the 0th order term, and 1.8 / 2.5 / 4 Hz/m for the x / y / z directions. The higher value on z is probably due to breathing during sampling, which is almost twice as long for this protocol than for the one used in the rest of the study (which uses partial Fourier).